

Velocity distributions of multi-ion species in an expanding plasma produced by a 1.05- μm laser

S. Sakabe, T. Mochizuki, T. Yabe, K. Mima, and C. Yamanaka
Institute of Laser Engineering, Osaka University, Suita, Osaka 565, Japan
(Received 22 January 1982)

The fast-ion-velocity distributions for polyethylene plasmas produced by spherical laser illumination were observed by a Thomson parabola spectrometer. It has been found that the velocity distributions have undulations, sharp truncations, and broad shelf structure because of multi-ion-species effects. The spherical symmetric plasma expansions including multi-ion-species and two-electron temperature effects have been simulated by a newly developed computer code. The simulation results indicate that protons are accelerated near the front edge of carbon ions, and the maximum velocity is determined predominantly by the ions which run in the region ahead of the carbon-ion front. Consequently, the proton-expansion front has a structure slipped out from the carbon-ion front towards vacuum. Since such protons compensate the accelerating electric field, the maximum velocities of proton and carbon ions become higher and lower, respectively, than in the case of single-ion species. These expansion dynamics reduced by the simulation can explain well the detailed structure of the observed velocity distribution.

I. INTRODUCTION

Fast-ion generation in laser-produced plasmas has been intensively investigated¹⁻³ because of the following reasons. A significant fraction of absorbed laser energy is considered to be carried out by fast ions and the fast-ion energy spectrum is useful for the electron-temperature measurements. In particular, it is important to know the multispecies fast-ion energy spectrum from laser-produced plasmas since an actual ablator like polyethylene contains several ion species.

The acceleration of cold ions by an electrostatic coupling with warm electrons has been studied theoretically by Gurevich *et al.*,⁴ who analytically derived a self-similar solution for the ion velocity with one electron temperature. At the laser intensities of the range 10^{14} – 10^{15} W/cm² at $\lambda = 1.05$ μm , however, the absorption process gives rise to a non-Maxwellian electron velocity distribution with a high-velocity tail.^{5,6} The electron velocity distribution is well known to be described by the superposition of a hot Maxwellian and a cold Maxwellian, and thus characterized by two electron temperatures. Wickens *et al.*⁷ derived a self-similar solution of expanding plasmas with two electron temperatures. They interpreted the slope of the ion-velocity distribution reduced from charge collector data by assuming the average charge number for ions. Although the charge collector with the time-of-flight

method is the simplest way to obtain the ion-velocity distribution, it is difficult to find the ion-velocity distribution for each ion species from charge collector data. The first explicit observations of ion-energy distributions from corona plasma containing multi-ion species have been done species separately using ion spectrometers by Decoste *et al.*^{8,9} and Joshi *et al.*¹⁰ The theoretical calculations of Gurevich and Wickens, which did not include multi-ion-species expansion and charge nonneutral effects, cannot explain the energy distribution obtained by Decoste *et al.* Decoste *et al.* modeled one-dimensional ambipolar plasma expansion of two-ion species in order to explain their experimental results. As the calculation results, in the case of a CH₂ target, the ratio of H⁺ and C⁶⁺ is increasing with ion energy, in qualitative agreement with the measured energy distributions. Additionally, they pointed out the existence of the mechanism that the expansion of the faster H⁺ ions decreases the electric-field strength such that the acceleration time and the electric field are essentially the same for both C⁶⁺ and H⁺. However, their calculations could explain only in part the multipeak structure in the energy distribution and the acceleration mechanism of multi-ion species. Although Widner *et al.* and Crow *et al.* studied charge-separation effects on single-ion-species plasma expansion numerically, charge-separation effects on multi-ion-species plasma expansion have not

been well understood.

In the following sections we present the experimental observation of undulations, sharp truncations, and broad shelf structure in the velocity distributions of the expanding ions from a laser-produced polyethylene plasma. The obtained ion distribution of each different ion is compared and discussed with computer simulation results which include non-neutral isothermal spherical expansion and two-electron-temperature effects.

II. EXPERIMENT AND RESULTS

In order to obtain velocity distributions for each ion species separately, we used a Thomson parabola ion spectrometer,¹² which was modified for obtaining a wide dynamic range. The details of this spectrometer have been described in Ref. 13. Here we will describe it briefly. Incident ions collimated by a pinhole are deflected by electric and magnetic fields. Deflections of the parallel direction (x) and the perpendicular direction (y) to the fields are proportional to the ratio of charge number to ion energy and that of charge number to ion momentum, respectively. The ions of a fixed A/Z value result in a single parabolic trace on the detector plane. On the detector surface (x - y) a straight line through the origin ($x=y=0$) corresponds to an isovelocity line. For obtaining a wide dynamic range, the electrodes of large gap were mounted in the down stream compared to the magnetic pole pieces, that is, these fields are never superposed, but separated spatially.

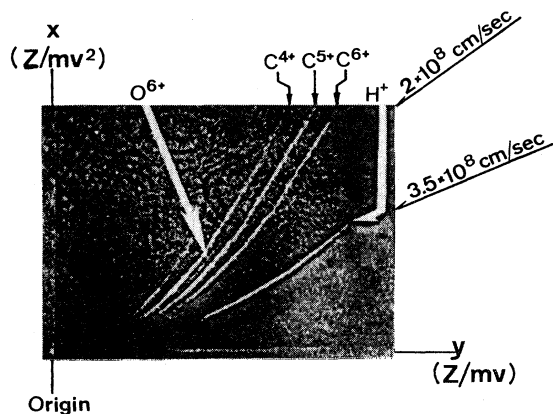


FIG. 1. Thomson parabola traces of the emitted ions from a $6\text{-}\mu\text{m}$ -thick $(\text{CH}_2)_n$ -coated glass microballoon target. Target was $100\ \mu\text{m}$ in diameter and irradiated by a $1.05\text{-}\mu\text{m}$ laser with the intensity of $10^{16}\ \text{W}/\text{cm}^2$ in 40 psec. Distance between a target and an entrance pinhole is 74 cm.

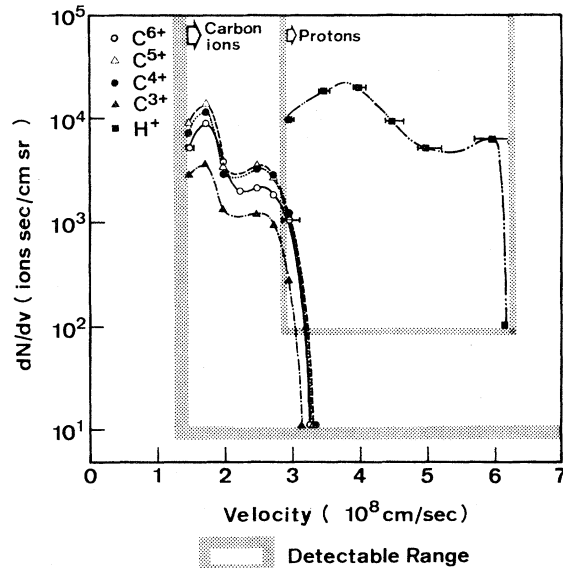


FIG. 2. Velocity distribution of fast ions reduced from the traces in Fig. 1. Regions enclosed by dots are the measurable range determined by the sensitivity and s/n ratio of a detector film.

A cellulose nitrate film (Kodak CA80-15) was used as an ion track detector.¹⁴ The track number ΔN in the limited area on the parabolic trace between isovelocity lines v and $v + \Delta v$ was carefully counted and then $\Delta N/\Delta v$ was calculated to result in the velocity distribution of each ion.

Figure 1 shows the ion parabolic traces obtained from a $6\text{-}\mu\text{m}$ -thick polyethylene-coated glass microballoon target irradiated symmetrically by a Gekko IV phosphate glass laser system with an incident energy of 102 J in 40 psec. Although the laser power density reached about $10^{16}\ \text{W}/\text{cm}^2$, full disintegration of the pellet shell of such thick coating takes a longer time compared with the time for ions to be accelerated up to ultrahigh velocities ($> 10^8\ \text{cm}/\text{sec}$). The traces of C^{6+} , C^{5+} , C^{4+} , C^{3+} , and H^+ were identified and an O^{6+} trace was found to exist between C^{5+} and C^{4+} traces. It is confirmed by separate shots that O^{6+} ions did not come from the glass microballoon, but impurity in the $(\text{CH}_2)_n$ -coated layer. Figure 2 shows the velocity distributions of fast ions reduced from these traces by the above-described method. Note in Figs. 1 and 2 the following points: (1) The velocity distribution of C^{6+} , C^{5+} , C^{4+} , and C^{3+} are similar to one another; (2) undulations exist on the distributions of carbon ions and protons; (3) the proton distribution shows a shelflike structure extending over the velocity range of about factor of 2 with a nearly constant dN/dv ; and (4) the distributions of carbon ions and protons

have sharp truncations at $v \simeq 3.3 \times 10^8$ cm/sec and $v \simeq 6.0 \times 10^8$ cm/sec, respectively.

From the first point, it is concluded that the fast ions observed are fully ionized in the early stage of acceleration and ionic charge number decreases by recombinations^{15,16} and/or charge exchanges¹⁷ with residual gas particles in the target chamber. Electron transfer to such highly ionized ions will take place dominantly at large impact parameters, so that a momentum change of the accelerated ions will be very small. Points (1) and (2) have also been observed by Decoste *et al.* To interpret (2)–(4), we developed a computer code EMI¹⁸ and simulated the results as it is described in the next section.

III. SIMULATION AND DISCUSSION

The charge separation at the expanding ion front plays a very important role for determining the high-energy tail of an ion-velocity distribution.^{19,20} Widner *et al.*²¹ studied single-ion-species acceleration by the Eulerian simulation code without assuming charge neutrality and showed that the ion density profile has a hump at the expansion front. A similar ion density structure at the front was also obtained analytically by Pearlman *et al.*²² On the other hand, Crow *et al.*¹¹ studied the plasma expansion by the Lagrange computer obtaining the ion density hump. However, they found that it decays during expansion (see Fig. 4 in Ref. 11). This might have come from the characteristics of the Lagrange computer code they used, because when the Lagrange code is applied to such expanding plasmas the computer mesh around the expansion front will generally become too large too rapidly to give accurate values during expansion. From Figs. 4 and 6 in Ref. 11, the obtained maximum velocity of the expanding ions seems to be given by the ions in the density dip behind the hump. These calculations were limited in a single-ion-species plasma expansion with one electron temperature and the velocity distributions were not explicitly shown. Pearlman *et al.* showed that the velocity maxima existed for the observed ions. They pointed out that nonneutral electrostatic sheath and/or a truncated non-Maxwellian electron velocity distribution at the critical density would be responsible for this limitation of the velocity. Such truncation will originate in the wave breaking mechanism that is believed to accompany resonant absorption. From the comparison with their experimentally observed truncation velocity of ions in laser-produced $(\text{CH}_2)_n$ plasmas, they concluded that the latter would be more dom-

inant. However, their value of the truncation velocity for protons was exactly the same as that for carbon ions.²² They assumed the predominant plasma species was C^{6+} and estimated the electron temperature from a charge collector signal. In addition, the laser power was 10^{14} W/cm² where the resonant absorption was negligible and the wave breaking was less probable.

In the present experiment, the protons' truncation velocity was about two times as large as that of carbon ions. The present experimental results including the protons' velocity distribution can not be fully interpreted by the frameworks of the studies described above.

In order to explain the feature of the experimentally obtained ion-velocity distributions, we developed an Eulerian code EMI to simulate the plasma expansion. A Lagrange code can not be applied to multi-ion-species plasma expansion since meshes for different ion species overlap.

In our computer calculation using the code EMI, the spherically symmetric multi-ion-species plasma expansion was simulated using a fluid model for the ions and the Boltzmann distributions both for the cold and hot electrons. The charge non-neutral effect was taken into account. Laser-produced plasmas have a source of energy so that the isothermal model will be a fair approximation. The equations to be solved numerically are as follows: equations of continuity

$$\frac{\partial n_j}{\partial t} + \frac{1}{r^2} \frac{\partial}{\partial r} (r^2 n_j v_j) = 0, \quad (1)$$

equations of motion

$$m_j \left[\frac{\partial v_j}{\partial t} + v_j \frac{\partial v_j}{\partial r} \right] = -Z_j e \frac{\partial \phi}{\partial r}, \quad (2)$$

Poisson's equation

$$\frac{1}{r^2} \frac{\partial}{\partial r} \left[r^2 \frac{\partial \phi}{\partial r} \right] = e \left(n_e - \sum_j Z_j n_j \right), \quad (3)$$

and electron density distribution

$$n_e = n_c + n_h = n_{c0} \exp \left[\frac{e\phi}{kT_c} \right] + n_{h0} \exp \left[\frac{e\phi}{kT_h} \right]. \quad (4)$$

Here, j refers to ion species and n_j , v_j , m_j , and Z_j are the density, velocity, mass, and charge number of ion j , respectively. ϕ is the electrostatic potential. n_e , n_c , and n_h are the densities of total electron, cold electron with temperature T_c , and hot electron with temperature T_h , respectively, and k is

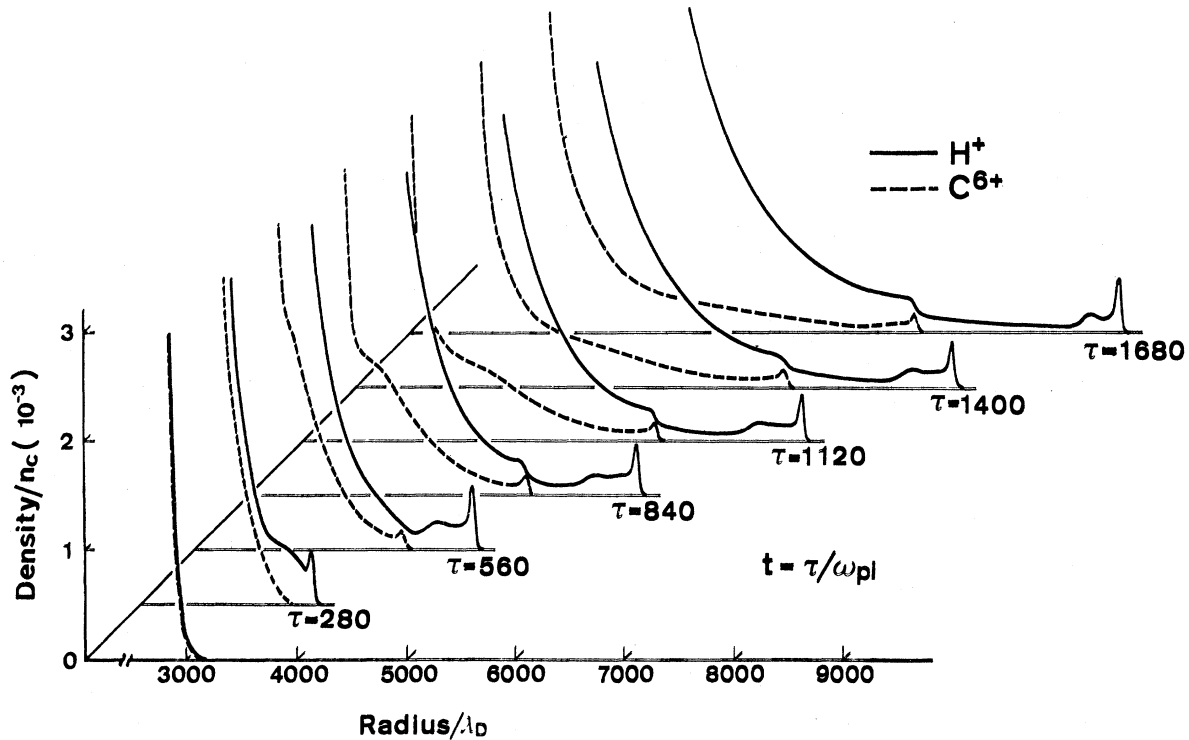


FIG. 3. Computer simulation results of H^+ and C^{6+} ion expansions. Model assumes the isothermal expansion and a Boltzmann distribution with two electron temperatures under the condition of $T_h/T_c=20$ and $n_c/n_h=70$.

the Boltzmann constant. Actual source plasma is approximated by a plasma sphere in the present code. The initial ion density profile is assumed to be a constant density sphere with a tail of scale length L , that is,

$$n_j(0,r) = \begin{cases} n_{j0}, & r \leq r_s \\ n_{j0} \exp\left(-\frac{r-r_s}{L}\right), & r \geq r_s. \end{cases}$$

The potential is chosen to be zero in the undisturbed plasma inner of the sphere since the undisturbed plasma is neutral. Thus, for the velocity and potential, initial and boundary values are

$$\begin{aligned} v_j(0,r) &= 0, \\ \Phi(0,r_1) &= 0, \\ \frac{\partial \Phi}{\partial r} \Big|_{r=r_1} &= \frac{\partial \Phi}{\partial r} \Big|_{r=r_2} = 0, \quad r_1 \leq r \leq r_2. \end{aligned}$$

A finite region of space between r_1 and r_2 was employed for the computations. In the present case the polyethylene target provides protons and carbon ions, which we refer to as $j=1$ and 2 , respectively. Since the density ratio of hydrogen atoms to carbon atoms in actual polymerized ethylene for the pellet

coating was found to be about 1.3–1.5, the initial density ratio of H^+ to C^{6+} is assumed to be 1.3 in the present simulation; $Z_1=1$ and $Z_2=6$. The initial ion density profile having a tail of scale length of L means that very low-level background ions will exist ahead of the ion front. This is a good approximation to the experimental situation since the hot electron and/or x-ray emission from the source plasma will have ionized some molecules of the rest gases in the vacuum chamber before the ion front propagates. Scale length L was assumed to be 60 times λ_D where λ_D is a Debye length at the critical density. Hot-electron temperature T_h was assumed to be about 10 keV, which is the experimentally given value by x-ray measurement. r_s was set to be $2550\lambda_D$ corresponding to the radius $60 \mu\text{m}$ of a pellet used in the experiment. However, the value of r_s was found to be insensitive to the feature of expansion. The boundary of calculation regions r_1 and r_2 were set at $2000\lambda_D$ and $10550\lambda_D$, respectively.

Figure 3 shows the calculated results for the ion density profile in polyethylene plasma expansion. τ is a normalized time by ω_{pi}^{-1} , where ω_{pi} is an ion plasma frequency for proton at the cutoff density. n_c is the cutoff density for 1.05- μm laser light. T_h/T_c and n_c/n_h were taken to be 20 and 70,

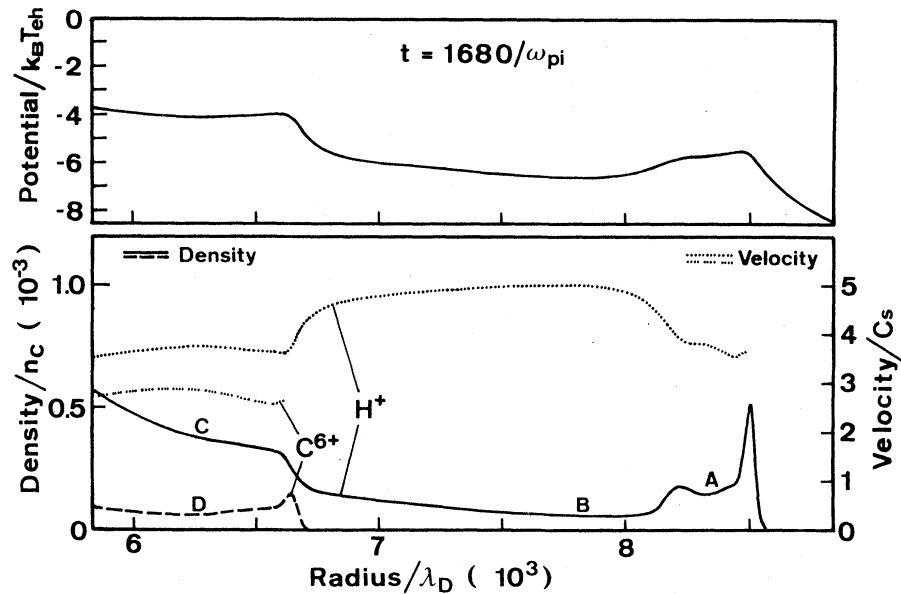


FIG. 4. Details of ion density, velocity profile, and the electrostatic potential profile near the ion expanding front at $t = 1680\omega_{pi}^{-1}$.

respectively. It is concluded that a quasineutral plasma exists at the region behind the ion fronts and the curves in this quasineutral region resemble the exponential form of the self-similar solution. The overall time behavior of the ion density profile in Fig. 3 shows that the protons are more effectively accelerated than the carbon ions. This can be easily imagined from the fact that the charge to mass ratio Z/M is twice as large for H^+ as for C^{6+} . Consequently, the proton-expansion front has a structure slipped out from the carbon-expansion front. Both density profiles obtained of the proton- and carbon-ion-expansion fronts are very similar to those found by Widner *et al.* and Pearlman *et al.* It is, however, interesting to note that the proton profile has the second hump just behind the front and the third hump at the carbon-ion front. The low-level background ions will be set in an acceleration state as soon as the ion front arrives, and contribute to the diffused shape of the ion front head.

For an understanding of the process to determine the feature of the generated fast ions ($v > 10^8$ cm/sec), the details of the ion velocities, ion densities, and potential profiles were calculated at $t = 1680/\omega_{pi}$, the end of the laser pulse, as shown in Fig. 4. The distribution of the faster plasma ion velocities will be approximately retained in subsequent expansion because the flow is quite supersonic and thus incapable of having a significant effect on the final ion velocities with rapidly decreasing electron

supply from the source plasma. It is clear that the potential is changing rapidly near the front of each ion species and charge neutrality breaks down at these places. The maximum velocities exist for protons and carbon ions, respectively. The proton maximum velocity is determined predominantly from the ions which run in region B in Fig. 4 after being accelerated near the front head of carbon ions, and not from the front head of protons. The carbon ions having the maximum velocity are contributed by that area in a wide region from D to the front head. It should be noted that computational results are based on the Boltzmann distribution for the electron. The Boltzmann relation is approximately valid until the ion velocity becomes comparable with the electron thermal velocity. But this distribution is not exact in the sense that unidirectionally streaming electrons like hot electrons generated at the critical density region of the source plasma will be reflected if they have smaller energies than a negative potential barrier, and therefore when a potential cavity region to trap electrons appears in an acceleration path, the real electron number density will be smaller there than that predicted by Boltzmann distribution. Such local reduction of the electron density may have an effect on ion velocities obtained in the present calculation. However, the obtained potential curve has a cavity in a small fraction of the acceleration region whose depth is only as high as 15% of the local potential height.

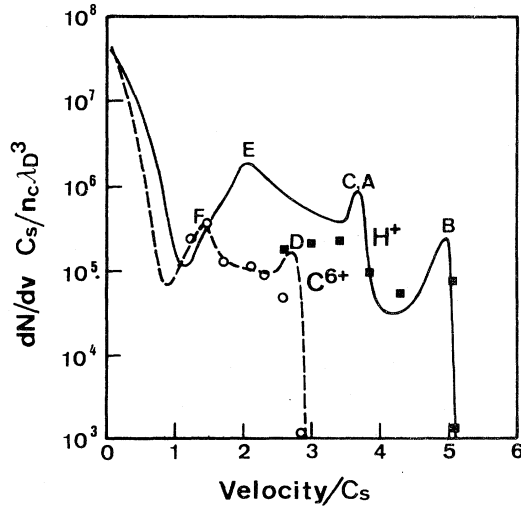


FIG. 5. Velocity distribution calculated from the simulation results in Fig. 3, and the experimental results. Number of carbon ions has been summed over $C^{6+} - C^{3+}$ ions.

Collision effects will diffuse the reduction described above. From these facts and the good agreement between the experimental results and simulation results, which we will describe next, we think such a non-Boltzmann effect does not reign the process in the present case.

Detailed study of the calculated density profile and velocity distribution at the earlier expansion stage of $\omega_{pi}t = 10 \sim 100$ showed that they already appear at these times in intrinsically similar forms to those in Fig. 4. The density profile of a high-

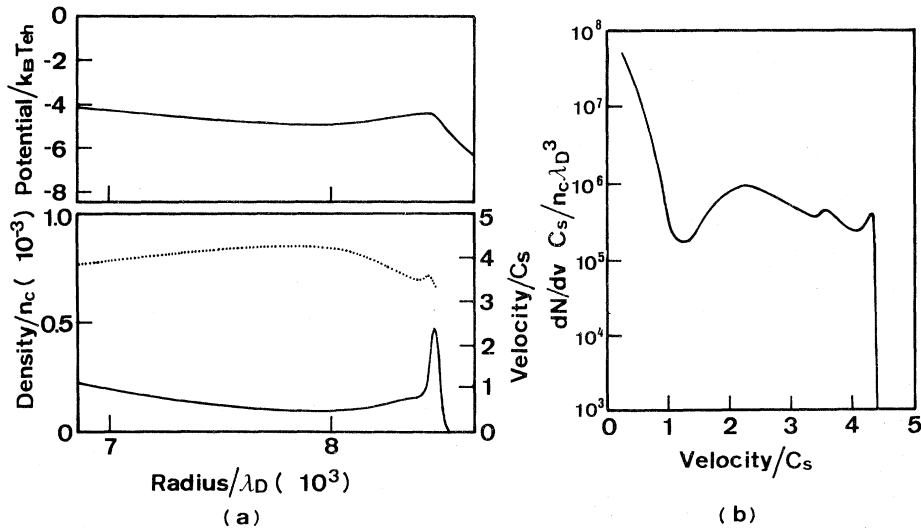


FIG. 7. (a) Ion density, velocity, and the potential profile near the expanding front ($t = 1680/\omega_{pi}$), and (b) the velocity distribution in the case where only protons exist as accelerated ions, under the condition $T_h/T_c = 20$, $n_c/n_h = 70$.

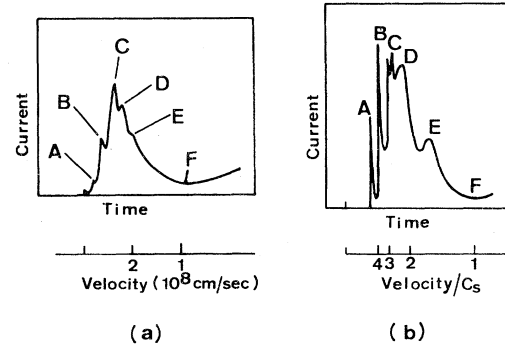


FIG. 6. Current signal experimentally observed by a charge collector (a), and the simulated signal (b).

density region is coincident with the self-similar solution and the calculated velocity distribution provides a velocity hump pertinent to the two-electron-temperature self-similar solution as discussed later. In order to assure the applicability of the present computer code, simulations on a single-ion-species plasma expansion were carried out at one-dimensional geometry. In these calculations it was found that the feature of plasma expansion at very early stages depends on the initial boundary condition, but thereafter the maximum ion velocity increases logarithmically with time, in a very similar manner to Crow's result, in the same range of $\omega_{pi}t$ they studied. The difference was the weak dependence of the slope in the maximum velocity-logarithmic time diagram on the initial boundary condition. It is therefore likely that the obtained velocity and density features at the front are not

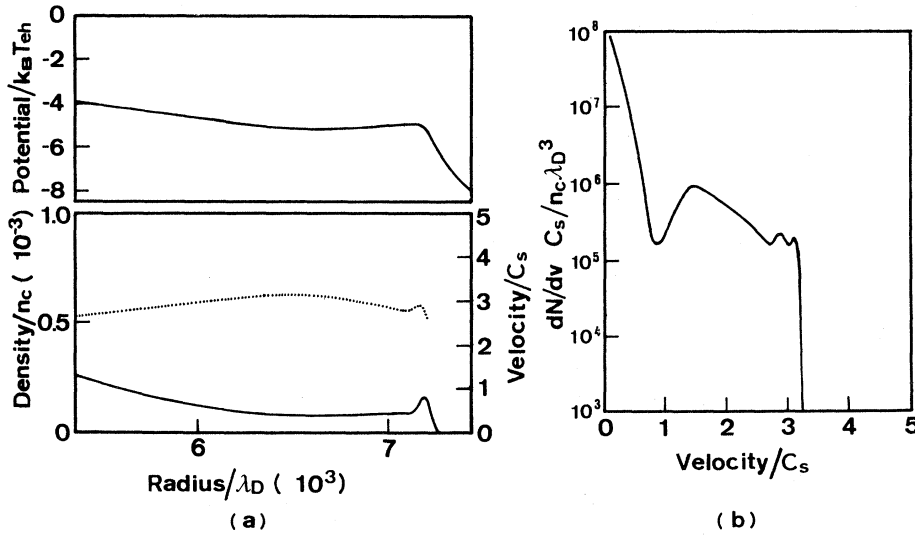


FIG. 8. (a) Ion density, velocity, and the potential profile near the expanding front ($t = 1680/\omega_{pi}$), and (b) the velocity distribution in the case where only carbon ions exist as accelerated ions, under the condition $T_h/T_c = 20$, $n_c/n_h = 70$.

due to the numerical errors of the present Eulerian code calculation. A more exact calculation will be given by taking into account the truncated non-Maxwellian electron-velocity distribution which might be given rise to in the present experimental condition.

The ion-velocity distribution was obtained from the result in Fig. 3 as follows. Detection at the detector position, that is sufficiently far from the source plasma, will provide the values of ion density $n_j(t_0, r)$ and velocity $v_j(t_0, r)$ where t_0 is a laser pulse duration. The number ΔN of ions between r and $r + \Delta r$ is

$$\Delta N = 4\pi r^2 \Delta r n_j(t_0, r).$$

The velocity distribution is then given by

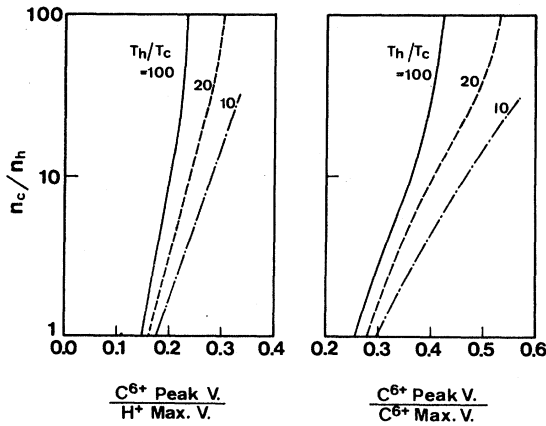


FIG. 9. Diagram of n_c/n_h vs R_1 and R_2 as a function of constant T_h/T_c value.

$$\frac{\Delta N}{\Delta v} = 4\pi r^2 n_j(t_0, r) \frac{\Delta r}{\Delta v},$$

$$v = v_j(t_0, r).$$

Figure 5 shows the velocity distribution calculated by the above method from the result at $t_0 = 1680\omega_{pi}^{-1}$, which corresponds to the experimental condition of a 40-psec laser pulse width in Fig. 3. A , B , C , and D correspond to the contributions from the ions at the same references in Fig. 4. The solid boxes and open circles correspond to experimental values of protons and carbon ions, respectively. Carbon ions were summed over $C^{6+} - C^{3+}$ numbers. The simulation result can well explain

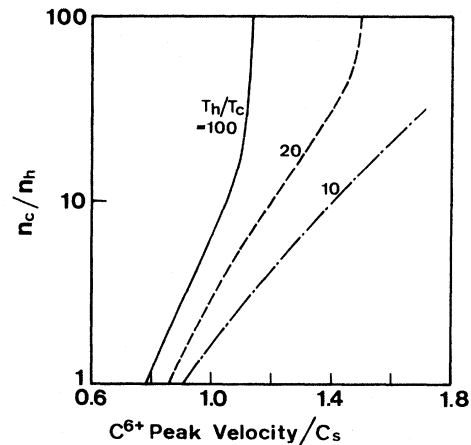


FIG. 10. Simulation relation between the C^{6+} peak velocity and ion sound velocity $C_s = \sqrt{T_h/m}$ as a function T_h/T_c .

TABLE I. Experimental values of characteristic velocity and T_h , T_c , and n_c/n_h value simulated. Simulated values are denoted by the superscript a.

C^{6+} peak velocity	V_{C_p}	$(1.75 \pm 0.05) \times 10^8$ cm/sec
C^{6+} maximum velocity	V_{C_m}	$(3.3 \pm 0.10) \times 10^8$ cm/sec
H^+ maximum velocity	V_{H_m}	$(6.0 \pm 0.20) \times 10^8$ cm/sec
Ratio V_{C_p}/V_{H_m}	R_1	0.29 ± 0.02
Ratio V_{C_p}/V_{C_m}	R_2	0.53 ± 0.03
Temperature ratio ^a	T_h/T_c	$15 \sim 20 \sim 30$
Density ratio ^a	n_c/n_h	$25 \sim 70 \sim 200$
C^{6+} peak velocity/ C_s ^a		$1.3 \sim 1.5 \sim 1.6$
Electron temperature ^a	T_h	$12.0 \sim 13.6 \sim 19.2$ keV
	T_c	$0.4 \sim 0.68 \sim 1.28$ keV

the experimental results, especially the humps in the distribution and the sharp truncation for both ions and the extending shelf structure of proton distribution. It is concluded that the humps *E* and *F* are due to the effect of two electron temperatures as reported by Wickens.⁷ Furthermore, to assume the existence of these humps, especially *A*, *B*, and *C* which appear in the calculated velocity distribution of Fig. 5, the distribution curves were transformed to time-of-flight spectra and summed over to give a current signal of a charge collector. The calculated current signal also shows several peaks corresponding to their respective humps described above, and its envelope is in fairly good agreement with that observed experimentally at a similar experimental condition as shown in Fig. 6.

Figure 7 shows the structure of the ion front (a) and the ion-velocity distribution (b) when only protons exist and Fig. 8 shows them when only carbon ions exist. In both cases, the initial ion density was adjusted to have the same value as that of polyethylene's case in Fig. 4, and other plasma parameters were fixed. It is seen that the profile of the density and velocity distribution are similar in

Figs. 7 and 8, and the proton-velocity distribution does not have as broad a shelf structure as shown in Fig. 5, and the truncation velocity (i.e., the maximum velocity) of protons is shifted towards lower velocity than that in the polyethylene expanding plasma. The truncation velocity of carbon ions is shifted towards higher velocity than that in the polyethylene expanding plasma. This will be due to the fact that there is no other coexisting and competing ion species like protons which will reduce the accelerating electric field.

Using parametric calculation results of the present simulation code, the electron temperatures T_c and T_h and the electron density n_c and n_h can be reduced from the experimentally obtained velocity distribution with some accuracy. In Fig. 9, the n_c/n_h is plotted against R_1 and R_2 as a function of constant T_h/T_c value where R_1 equals the ratio of C^{6+} peak (*E* in Fig. 4) velocity to H^+ maximum velocity and R_2 equals the ratio of C^{6+} peak velocity to C^{6+} maximum velocity. Figure 10 shows the simulation relation between the C^{6+} peak velocity and ion sound velocity $C_s = \sqrt{T_h/m}$ as a function of constant T_h/T_c , where m is proton mass. From the experimentally obtained values of R_1 and R_2 , we can determine both n_c/n_h and T_h/T_c simultaneously using the diagram in Fig. 9, and then T_h using that in Fig. 10. The experimentally obtained parameters and the plasma parameters determined according to the above-described process are summarized in Table I. Figure 11 shows T_h and T_c scaling against laser intensity which was determined by using x-ray spectroscopy for bremsstrahlung. T_h and T_c values in Table I are in a fairly good agreement with that inferred by Fig. 11.

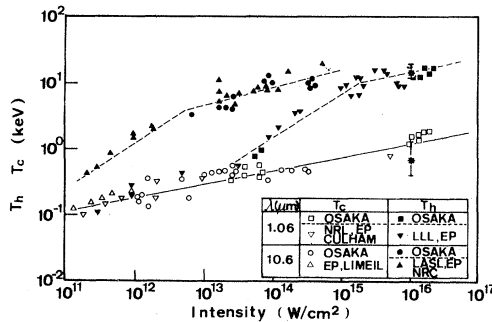


FIG. 11. Scaling of hot- and cold-electron temperatures as a function of laser fluence (Ref. 23). Asterisks correspond to the values obtained from the velocity distributions of fast ions.

IV. SUMMARY AND CONCLUSION

The velocity distributions of the fast ions emitted from laser-produced polyethylene plasmas were ob-

tained for defined ion species using the modified Thomson parabola spectrometer. It was found that undulations exist on the velocity distributions of carbon ions and protons and the proton distribution has a shelflike structure. The additional hump and shelflike structure observed can be explained neither by two-electron-temperature self-similar solutions nor by single-ion-species computer simulation results. Both distributions of protons and carbon ions have sharp truncations at different velocities. The former's truncation velocity was found to be about two times as large as the latter's. In order to interpret these features, the computer code EMI was developed. This code can simulate the spherically symmetric multi-ion species plasma expansion with two electron temperatures and in this code the charge nonneutral effect was taken into account. From comparison of the present simulations with the formerly obtained computer simulation at one dimension and with single-ion-species expansion, it seems likely that the velocity and density features at the expansion front obtained by this code are not

due to the numerical errors of this Eulerian code calculation. The present simulation result indicates the following. Protons are accelerated near the front edge of carbon ions and slipped out from the carbon-ion front towards the vacuum and the maximum velocity is determined predominantly by the ions which run in the ahead region of the carbon ion front. As a result, the maximum velocity of protons is higher than that in the single-ion-species case. On the contrary, the maximum velocity of carbon ions is lower, because protons compensate the accelerating electric field. These results give some insight on the dynamical feature of ion acceleration in expanding plasmas of multispecies components. The simulation results explained well the structure of the observed velocity distribution. From the comparison between the numerically parametrized results of these simulations and the experimental values of the ion velocity, the temperatures of both hot and cold electrons and their densities at the source plasmas have been determined with some accuracy.

-
- ¹E. J. Valeo and I. B. Bernstein, *Phys. Fluids* **19**, 1348 (1976).
- ²K. A. Brueckner and R. S. Janda, *Nucl. Fusion* **17**, 1265 (1977).
- ³P. M. Campbell, R. R. Johnson, F. J. Mayer, L. V. Powers, and D. C. Slater, *Phys. Rev. Lett.* **39**, 274 (1977).
- ⁴A. V. Gurevich, L. V. Pariiskaya, and L. P. Pitaevskii, *Zh. Eksp. Teor. Fiz.* **49**, 647 (1965) [*Sov. Phys.—JETP* **22**, 449 (1966)].
- ⁵W. C. Mead, R. A. Haas, W. L. Kruer, D. W. Phillion, H. N. Kornblum, J. D. Lindl, D. R. MacQuigg, and V. C. Rupert, *Phys. Rev. Lett.* **37**, 489 (1976).
- ⁶K. G. Estabrook and W. L. Kruer, *Phys. Rev. Lett.* **40**, 42 (1978).
- ⁷L. M. Wickens, J. E. Allen, and P. T. Rumsby, *Phys. Rev. Lett.* **41**, 243 (1978).
- ⁸R. Decoste and B. H. Ripin, *Phys. Rev. Lett.* **40**, 34 (1978).
- ⁹R. Decoste and B. H. Ripin, *Appl. Phys. Lett.* **31**, 68 (1977).
- ¹⁰C. Joshi, M. C. Richardson, and G. D. Enright, *Appl. Phys. Lett.* **34**, 625 (1977).
- ¹¹J. E. Crow, P. L. Auer, and J. E. Allen, *J. Plasma Phys.* **14**, 65 (1975).
- ¹²J. J. Thomson, *Philos. Mag.* **21**, 225 (1911).
- ¹³S. Sakabe, T. Mochizuki, T. Yamanaka, and C. Yamanaka, *Rev. Sci. Instrum.* **51**, 1314 (1980).
- ¹⁴R. L. Fleischer, P. B. Price, and R. M. Walker, *Nuclear Tracks in Solids* (University of California Press, Berkeley, 1975).
- ¹⁵R. R. Goforth and P. Hammerling, *J. Appl. Phys.* **47**, 3918 (1976).
- ¹⁶G. S. Vororov and L. E. Chernyshev, *Zh. Tekh. Fiz.* **43**, 1484 (1973) [*Sov. Phys.—Tech. Phys.* **18**, 940 (1974)].
- ¹⁷D. Rapp and W. E. Francis, *J. Chem. Phys.* **37**, 2631 (1962).
- ¹⁸S. Sakabe and T. Yabe, research report, Osaka University (unpublished).
- ¹⁹D. Montgomery, *Phys. Rev. Lett.* **19**, 1465 (1967).
- ²⁰B. Bezzerides, D. W. Forslund, and E. L. Lindmann, *Phys. Fluids* **21**, 2179 (1978).
- ²¹M. Widner, I. Alexeff, and W. D. Jones, *Phys. Fluids* **14**, 795 (1971).
- ²²J. S. Pearlman and R. L. Morse, *Phys. Rev. Lett.* **40**, 1652 (1978). In Table I, the values of 5.5 and 7.7 were given as the proton- and carbon-ion truncation velocities. Those values were normalized by the respective sound velocities, therefore the absolute values are identical.
- ²³C. Yamanaka, S. Nakai, Y. Kato, T. Sasaki, and T. Mochizuki, *Laser Interaction and Related Plasma Phenomena*, edited by H. J. Schwarz, H. Hora, H. Lubin, and B. Yaakobi (Plenum, New York, 1981), Vol. 5, p. 541.

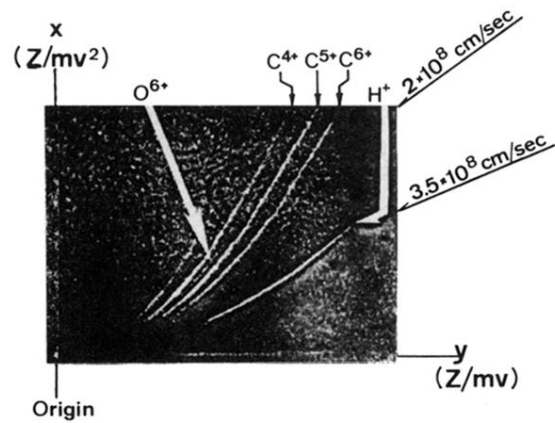


FIG. 1. Thomson parabola traces of the emitted ions from a $6\text{-}\mu\text{m}$ -thick $(\text{CH}_2)_n$ -coated glass microballoon target. Target was $100\ \mu\text{m}$ in diameter and irradiated by a $1.05\text{-}\mu\text{m}$ laser with the intensity of $10^{16}\ \text{W}/\text{cm}^2$ in 40 psec. Distance between a target and an entrance pinhole is 74 cm.